ITERATIVE QUASI-NEWTON SOLVERS FOR POROMECHANICS APPLIED TO HEART PERFUSION

N. Barnafi*, J. W. Both†

* Dipartimento di Matematica "F. Enriques"
Università degli Studi di Milano
Milan, Italy
nicolas.barnafi@unimi.it

† Department of Mathematics
University of Bergen
Bergen, Norway
jakub.both@uib.no

Key words: Poromechanics, Iterative solvers, Fixed-stress split, Biomedical application

Abstract: *In this work, the efficient approximation of a nonlinear cardiac poromechanics model is investigated. Quasi-Newton solvers based on iterative two-way and three-way decoupling are proposed. For increased robustness and better performance, the iterative schemes are accelerated by additionally using Anderson acceleration. The solvers are tested for a numerical example simulating cardiac perfusion. The results obtained demonstrate a significant speed-up for the splitting approaches with respect to the standard monolithic Newton method.*

1 INTRODUCTION

Cardiac perfusion describes the fundamental process of blood supply of the heart muscle, but its importance at the outset of cardiac disease remains largely understudied. This motivates the use of mathematical models to deepen the understanding of this phenomenon. The complex network structure of the coronary vessels in the heart and tissue itself (myocardium) have been mainly addressed by the use of poroelastic models [14, 9, 11], which possess the advantage of greatly reducing the complexity of the vessels through formal averaging techniques [20].

Nonlinear poroelasticity consists in a complex multi-physics model, whose numerical approximation is still under active research. The linear case, i.e. Biot's equation, is instead better understood, with iterative coupling strategies presenting the most successful family of methods for this kind of problem. The main ones used in practice are the undrained [21] and fixed-stress [16] splitting schemes. These methods alternate between solving for flow and then solid variables until convergence, while keeping the others fixed. For guaranteed robustness, however, sufficient stabilization has to be used which can be obtained through analysis. Computational costs may be significantly reduced due to the decoupling, which relies on solving many times simpler sub-problems instead of solving once a difficult problem. The concept of decoupling can be extended to nonlinear problems as a quasi-Newton method [15, 4, 5], where the computational cost reduction can become even more relevant.

In this work, we study the nonlinear solution of a simplified nonlinear model for cardiac poromechanics. The model combines thermodynamically-consistent linearization [7] of a fully-nonlinear model [10], but with a nonlinear constitutive stress-strain relation [13]; the final model consists in a nonlinear coupled system of three physics. Quasi-Newton solvers are proposed integrating stabilized two-way and three-way decoupling, inspired by splitting schemes derived for the linearized model [3] which guarantee linear convergence. Our numerical results show that our iterative splitting quasi-Newton schemes outperform the widely used monolithic Newton method, with a reduction in computer times of up to a 50% for the three-way and an 85% for the two-way, making them an attractive choice for the fully-nonlinear models.

https://doi.org/10.4995/YIC2021.2021.12324

2 NONLINEAR POROELASTICITY MODEL FOR CARDIAC PERFUSION

The scope of the following model is twofold: on one hand, it captures the interaction between the deformation of the myocardium during a heartbeat and the myocardial coronary vessels, and on the other hand it provides a simple scenario in which numerical methods can be tested. We pose our problem on a prolate ellipsoid geometry Ω representing a left ventricle, cf. Figure 2.

The poromechanics model we consider is given by the following: Find a displacement $\boldsymbol{y}_s$, absolute fluid velocity $\boldsymbol{v}_f$ and pressure p such that

$$\begin{aligned} \mathcal{F}_s &:= \rho_s(1-\phi)\partial_{tt}\boldsymbol{y}_s - \operatorname{div}\,\mathbf{P}(\mathbf{F},t) + (1-\phi)\,\nabla p - \phi^2\boldsymbol{\kappa}_f^{-1}\,(\boldsymbol{v}_f - \partial_t\boldsymbol{y}_s) = \mathbf{0} \quad \text{in } \Omega, \\ \mathcal{F}_f &:= \rho_f\phi\partial_t\boldsymbol{v}_f - \operatorname{div}\,(\phi\boldsymbol{\sigma}_{\text{vis}}(\boldsymbol{v}_f)) + \phi\,\nabla p + \phi^2\boldsymbol{\kappa}_f^{-1}\,(\boldsymbol{v}_f - \partial_t\boldsymbol{y}_s) = \mathbf{0} \quad \text{in } \Omega, \\ \mathcal{F}_p &:= \frac{(1-\phi)^2}{\kappa_{\text{s}}}\partial_t p + \operatorname{div}\,(\phi\boldsymbol{v}_f) + \operatorname{div}\,((1-\phi)\,\partial_t\boldsymbol{y}_s) = 0 \quad \text{in } \Omega, \end{aligned} \tag{1}$$

where $\boldsymbol{\sigma}_{\text{vis}} := 2\mu_f\boldsymbol{\varepsilon}(\boldsymbol{v}_f)$ and $\boldsymbol{P}$ is the Piola stress tensor, given by $\boldsymbol{P}(\boldsymbol{F},t) := \frac{d\Psi}{d\boldsymbol{F}} + \boldsymbol{P}_a(\boldsymbol{F},t)$ for a Helmholtz potential Ψ and an active stress tensor $\boldsymbol{P}_a(\boldsymbol{F},t)$, specified further below. The remaining parameters are: solid density ρ_s, fluid density ρ_f, porosity ϕ, permeability tensor $\boldsymbol{\kappa}_f$ and bulk modulus κ_s.

To model the ventricle mechanics, a Guccione fiber oriented constitutive law [13] was used together with an artificial active contraction force. The constitutive law is given by

$$\Psi(\boldsymbol{F}) := C\exp\{Q(\boldsymbol{F})-1\} + \frac{\kappa}{2}(J-1)\log J, \tag{2}$$

$$Q := b_f E_{ff}^2 + b_s E_{ss}^2 + b_n E_{nn}^2 + 2(b_{fs}E_{fs}^2 + b_{fn}E_{fn}^2 + b_{sn}E_{sn}^2), \tag{3}$$

$$\boldsymbol{E} := \frac{1}{2}(\boldsymbol{F}^T\boldsymbol{F} - \boldsymbol{I}),\ \boldsymbol{F} = \nabla\,\boldsymbol{y}_s + \boldsymbol{I},\ J := \det(\boldsymbol{F}),\ E_{uv} := (\boldsymbol{E}\boldsymbol{v})\cdot\boldsymbol{u}, \tag{4}$$

where $\boldsymbol{f}, \boldsymbol{s}$ and $\boldsymbol{n}$ are a pointwise set of independent vectors directed towards the heart fibers, sheets and normal directions, and the active stress is given by

$$\boldsymbol{P}_a(\boldsymbol{F},t) := 3\cdot 10^4\,\sin(\pi t)\frac{(\boldsymbol{F}\boldsymbol{f})\otimes\boldsymbol{f}}{\|\boldsymbol{F}\boldsymbol{f}\|}. \tag{5}$$

We use the same parameters from [18]: $C = 0.88\cdot 10^3, b_f = 8, b_s = 6, b_n = 3, b_{fs} = 12, b_{fn} = 3, b_{sn} = 3, \kappa = 5\cdot 10^4$ for the nonlinear constitutive law, and the ones from [7] for the remaining parameters: $\rho_f = \rho_s = 10^3$, $\phi = 0.1$, $\boldsymbol{\kappa}_f = 10^{-7}$ and $\kappa_s = 10^8$. All parameters are considered within the SI unit system.

We note that this is a hybrid model, in the sense that it includes a nonlinear mechanics response but it does not account for large deformations in the fluid momentum and mass conservation. Still, it correctly captures the deformation pattern of a beating heart and, as our results show, provides an adequate framework for studying the interaction strength between the mechanics and the porous media flow. We thereby expect conclusions of this work to be also applicable to extended models.

2.1 Initial and boundary conditions

The initial conditions are simply given by

$$\boldsymbol{y}_s(0) = \boldsymbol{y}_{s0},\quad \partial_t\boldsymbol{y}_s(0) = \boldsymbol{v}_{s0},\quad \boldsymbol{v}_f(0) = \boldsymbol{v}_{f0},\quad p(0) = p_0. \tag{6}$$

The boundary conditions are defined as follows: the mechanics follow the Robin boundary conditions from [18] which model the interaction with the pericardium at both the epicardium

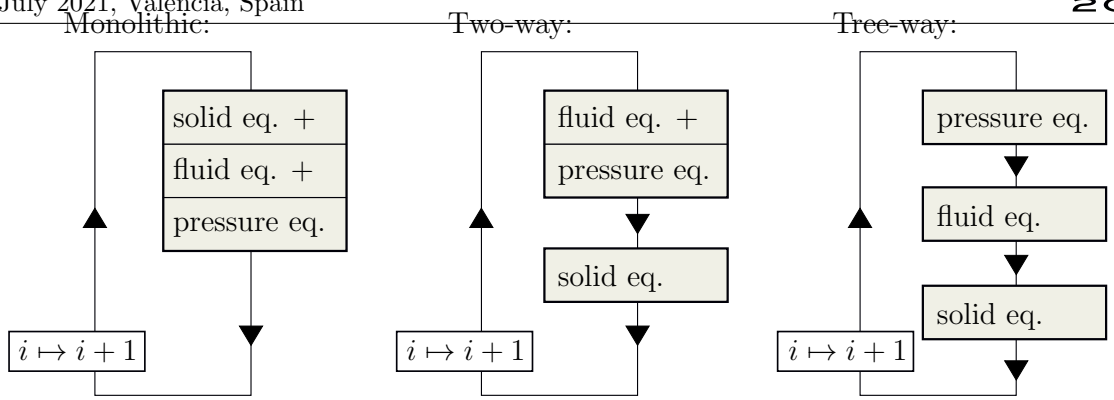

Figure 1: Summary of the monolithic, two-way, and three-way split solver strategies at an arbitrary iteration i, where connected blocks denote coupled physics.

(external surface) and the base (circular ring on top), whereas the endocardium (inner surface) uses a null Neumann condition. For the blood we consider a no-slip condition $\boldsymbol{v}_f = \partial_t \boldsymbol{y}_s$ on the endocardium and epicardium, and at the base of the heart we set a null Neumann condition which allows for the blood to freely leave the tissue.

2.2 Numerical discretization

We use the continuous Galerkin finite element method for solving this problem. For this, we consider the inf-sup stable family of generalized Taylor-Hood elements $\mathbb{P}_2 \times \mathbb{P}_2 \times \mathbb{P}_1$ [2] for the solid×fluid×pressure space, and we use an implicit Euler method with a fixed time-step Δt. We note that this approach is equally valid for the energy-consistent discretization shown in [6], as well as higher order methods. The no-slip condition is imposed weakly as in [6].

The use of higher order finite elements for the displacement, although less frequently used in the mechanics community, are common practice in the field of geomechanics, requiring an inf-sup stability condition for the displacement and pressure finite element spaces. Yet, we note that such discretization has also already been used in the context of cardiac poromechanics [11]. This relation is also true for the linear model we used as a base for our hybrid model, with the inf-sup constant being proportional to the solid porosity $1 - \phi$ for the case in which the displacement is approximated with the lower order $\mathbb{P}_1$ elements [2].

3 MONOLITHIC AND BLOCK-PARTITIONED NUMERICAL SOLVERS

We present three iterative solver strategies for solving the nonlinear problem from Section 2: a monolithic, a two-way splitting, and a three-way splitting approach, outlined in Fig. 1. The monolithic scheme is the standard Newton method, whereas the splitting schemes are formulated as quasi-Newton solvers, i.e. each iteration is a linearization iteration decoupling different physical sub-problems by a suitable choice of the inexact Jacobian. The decoupling strategies are closely related to previous developments for the corresponding linearized problem [3].

Through simultaneous linearization and decoupling, a significant reduction in overall computational cost can be expected as observed for other nonlinear poroelasticity problems [4]. Furthermore, we suggest employing Anderson acceleration to both improve the performance and slightly relax the need for well-chosen stabilization parameters.

All solvers are formulated in residual form, allowing in particular for a direct comparison. For this, we denote with $\mathcal{F}_s$, $\mathcal{F}_f$, and $\mathcal{F}_p$ the canonical residuals of the solid momentum, fluid momentum, and mass conservation/pressure equations, respectively. Throughout the remaining section, i will denote the current iteration index which decorates approximations, e.g. $\boldsymbol{y}_s{}^i$, as well as increments, e.g., $\delta \boldsymbol{y}_s{}^i$.

The resulting schemes consider at each iteration i some approximation $(\boldsymbol{y}_s{}^i, \boldsymbol{v}_f^i, p^i)$, for which

we compute an increment $(\delta \boldsymbol{y}_s{}^i, \delta \boldsymbol{v}_f{}^i, \delta p^i)$. The next iteration is then defined by $(\boldsymbol{y}_s{}^{i+1}, \boldsymbol{v}_f^{i+1}, p^{i+1}) := (\boldsymbol{y}_s{}^i, \boldsymbol{v}_f^i, p^i) + (\delta \boldsymbol{y}_s{}^i, \delta \boldsymbol{v}_f{}^i, \delta p^i)$. In the following, we specify the definition of the different linearization steps.

3.1 Monolithic Newton solver

The monolithic Newton solver is usually the first-choice linearization scheme for nonlinear problems (see [12] for the case of cardiac mechanics). The Jacobian is given by a full linearization of the governing equations (1) after discretization.

The linearization step at iteration $i \geq 0$ reads: Compute $(\delta \boldsymbol{y}_s{}^i, \delta \boldsymbol{v}_f{}^i, \delta p^i)$ such that

$$\frac{\rho_s(1-\phi)}{\Delta t^2}\delta \boldsymbol{y}_s{}^i - \operatorname{div}\, \partial_{\boldsymbol{y}_s} \boldsymbol{P}(\boldsymbol{F}^i) : \delta \boldsymbol{y}_s{}^i + (1-\phi)\,\nabla\, \delta p^i \\ -\phi^2 \boldsymbol{\kappa}_f^{-1}\left(\delta \boldsymbol{v}_f{}^i - \frac{\delta \boldsymbol{y}_s{}^i}{\Delta t}\right) = -\mathcal{F}_s(\boldsymbol{y}_s{}^i, \boldsymbol{v}_f^i, p^i), \tag{7}$$

$$\frac{\rho_f \phi}{\Delta t}\delta \boldsymbol{v}_f{}^i - \operatorname{div}\, \left(\phi \boldsymbol{\sigma}_{\text{vis}}(\delta \boldsymbol{v}_f{}^i)\right) + \phi\,\nabla\, \delta p^i \\ +\phi^2 \boldsymbol{\kappa}_f^{-1}\left(\delta \boldsymbol{v}_f{}^i - \frac{\delta \boldsymbol{y}_s{}^i}{\Delta t}\right) = -\mathcal{F}_f(\boldsymbol{y}_s{}^i, \boldsymbol{v}_f^i, p^i), \tag{8}$$

$$\frac{(1-\phi)^2}{\kappa_{\text{s}} \Delta t}\delta p^i + \operatorname{div}\, \left(\phi \delta \boldsymbol{v}_f{}^i\right) + \operatorname{div}\, \left((1-\phi)\,\frac{\delta \boldsymbol{y}_s{}^i}{\Delta t}\right) = -\mathcal{F}_p(\boldsymbol{y}_s{}^i, \boldsymbol{v}_f^i, p^i), \tag{9}$$

Algebraically, this can be written as

$$\begin{bmatrix} \boldsymbol{D}_{\boldsymbol{y}_s}\boldsymbol{R}_s^i & \boldsymbol{A}_{fs}^\top & -\boldsymbol{B}_s^T \\ \boldsymbol{A}_{fs} & \boldsymbol{A}_f & -\boldsymbol{B}_f^T \\ \boldsymbol{B}_s & \boldsymbol{B}_f & \boldsymbol{A}_p \end{bmatrix} \begin{bmatrix} \boldsymbol{\delta y_s}{}^i \\ \boldsymbol{\delta v_f}{}^i \\ \boldsymbol{\delta p}^i \end{bmatrix} = - \begin{bmatrix} \boldsymbol{R}_s^i \\ \boldsymbol{R}_f^i \\ \boldsymbol{R}_p^i \end{bmatrix}, \tag{10}$$

with natural definitions of the block matrices $\boldsymbol{A}_{(\cdot)(\cdot)}, \boldsymbol{B}_{(\cdot)}$ and residual vectors $\boldsymbol{R}_{(\cdot)}$. The monolithic solver strategy does not utilize the fact that all blocks aside of the solid diagonal block $\boldsymbol{D}_{\boldsymbol{y}_s}\boldsymbol{R}_s^i$ are constant. Splitting solvers are instead capable of making use of all constant blocks, i.e. $\boldsymbol{A}_{(\cdot)(\cdot)}$ and $\boldsymbol{B}_{(\cdot)}$.

3.2 Two-way splitting

We employ ideas previously developed for the linearized problem [3] justified by a similar coupling character of the exact Jacobian, cf. Sec. 3.1. For this, the mechanics equations are decoupled from the remaining two equations, and the mass conservation equation is stabilized with a weighted L^2-type term – essentially as in the fixed-stress split for Biot's equations.

Let β_p denote a user-defined stabilization parameter, and associate a weighted L^2-type bilinear form $(p, q) \mapsto \beta_p \langle p, q \rangle_{L^2}$ with a corresponding discretization matrix $\boldsymbol{S}_p$. Then the two-way split is given by a decoupled solver with diagonal L^2-type stabilization, which can be written algebraically at each iteration i as: Find the increment $(\boldsymbol{\delta y_s}{}^i, \boldsymbol{\delta v_f}{}^i, \boldsymbol{\delta p}^i)$ satisfying

$$\begin{bmatrix} \boldsymbol{D}_{\boldsymbol{y}_s}\boldsymbol{R}_s^i & \boldsymbol{A}_{fs}^\top & -\boldsymbol{B}_s^T \\ \boldsymbol{0} & \boldsymbol{A}_f & -\boldsymbol{B}_f^T \\ \boldsymbol{0} & \boldsymbol{B}_f & \boldsymbol{A}_p + \boldsymbol{S}_p \end{bmatrix} \begin{bmatrix} \boldsymbol{\delta y_s}{}^i \\ \boldsymbol{\delta v_f}{}^i \\ \boldsymbol{\delta p}^i \end{bmatrix} = - \begin{bmatrix} \boldsymbol{R}_s^i \\ \boldsymbol{R}_f^i \\ \boldsymbol{R}_p^i \end{bmatrix} \tag{11}$$

Equivalently, the two-way split can be performed in two separate steps. First the coupled fluid momentum and stabilized mass conservation equations are solved. Second, the solid

momentum equation is solved with updated fluid flow parameters. We highlight that the first step does not require any setup update over the course of iterations.

For the linearized problem, convergence can be showed for a range of stabilization values [3]. We expect similar robustness in the nonlinear case.

3.3 Three-way splitting

The two-way split still involves the solution of the coupled fluid momentum and mass conservation equations, which have the character of a time-dependent Stokes equations. Inspired by developments for the time-dependent Stokes equations [8], we apply additional decoupling with two sub-steps accounting for one of the two contributions (L^2-type and diffusion-type) in the fluid velocity diagonal block $\boldsymbol{A}_f$. Similarly to the fixed-stress split, the diffusion contribution in $\boldsymbol{A}_f$ suggests an L^2-type stabilization $\boldsymbol{S}_{CC,mass}$, associated to $(p,q) \mapsto \beta_{CC,mass}\langle p,q\rangle_{L^2(\Omega)}$, whereas the L^2-type contribution in $\boldsymbol{A}_f$ results in a Laplace-type stabilization $\boldsymbol{S}_{CC,diff}$, associated with $(p,q) \mapsto \beta_{CC,diff}\langle \nabla p, \nabla q\rangle_{L^2(\Omega)}$. Here, $\beta_{CC,mass}$ and $\beta_{CC,diff}$ denote two (additional) user-defined stabilization parameters.

The total increment is then obtained through mixing with parameter $\gamma \in [0,1]$

$$(\delta \boldsymbol{y_s}^i, \delta \boldsymbol{v_f}^i, \delta p^i) \coloneqq \gamma(\delta \boldsymbol{y_s}^i_{mass}, \delta \boldsymbol{v_f}^i_{mass}, \delta p^i_{mass}) + (1-\gamma)(\delta \boldsymbol{y_s}^i_{diff}, \delta \boldsymbol{v_f}^i_{diff}, \delta p^i_{diff}) \tag{12}$$

where the two increments are computed by solving the three-way splitting methods

$$\begin{bmatrix} \boldsymbol{D}_{\boldsymbol{y}_s}\boldsymbol{R}_s^i & \boldsymbol{A}_{fs}^\top & -\boldsymbol{B}_s^T \\ \boldsymbol{0} & \boldsymbol{A}_f & -\boldsymbol{B}_f^T \\ \boldsymbol{0} & \boldsymbol{0} & \boldsymbol{A}_p + \boldsymbol{S}_p + \boldsymbol{S}_{CC,mass} \end{bmatrix} \begin{bmatrix} \boldsymbol{\delta y_s}^i_{mass} \\ \boldsymbol{\delta v_f}^i_{mass} \\ \boldsymbol{\delta p}^i_{mass} \end{bmatrix} = - \begin{bmatrix} \boldsymbol{R}_s^i \\ \boldsymbol{R}_f^i \\ \boldsymbol{R}_p^i \end{bmatrix}, \tag{13}$$

and

$$\begin{bmatrix} \boldsymbol{D}_{\boldsymbol{y}_s}\boldsymbol{R}_s^i & \boldsymbol{A}_{fs}^\top & -\boldsymbol{B}_s^T \\ \boldsymbol{0} & \boldsymbol{A}_f & -\boldsymbol{B}_f^T \\ \boldsymbol{0} & \boldsymbol{0} & \boldsymbol{A}_p + \boldsymbol{S}_p + \boldsymbol{S}_{CC,diff} \end{bmatrix} \begin{bmatrix} \boldsymbol{\delta y_s}^i_{diff} \\ \boldsymbol{\delta v_f}^i_{diff} \\ \boldsymbol{\delta p}^i_{diff} \end{bmatrix} = - \begin{bmatrix} \boldsymbol{R}_s^i \\ \boldsymbol{R}_f^i \\ \boldsymbol{R}_p^i \end{bmatrix}. \tag{14}$$

3.4 Choice of stabilization parameters and acceleration

The two-way and three-way splitting schemes involve the choice of user-defined stabilization parameters β_p, $\beta_{CC,mass}$, $\beta_{CC,diff}$, and a mixing parameter γ. In the numerical example in Section 4, inspired by the strategy in [17], we manually chose $\beta_p = 0.22$ as it resulted in the fewest iterations for the first 10 time steps. We keep the value fixed over the course of the entire simulation. The linear structure of the fluid-pressure coupling naturally suggests $\beta_{CC,mass} = 3\phi/(2\mu_f)$ and $\beta_{CC,diff} = \left(\rho_f(\Delta t)^{-1}\boldsymbol{I} + \boldsymbol{\kappa}_f^{-1}\right)^{-1}$. The mixing parameter is chosen as $\gamma = 0.9$ to favor the L^2-type stabilization.

The performance of the solvers depends on the choice of the parameters. However, the nonlinear character of the problem impedes optimization at each iteration; we note that the non-constant diagonal block $\boldsymbol{D}_{\boldsymbol{y}_s}\boldsymbol{R}_s^i$ in particular controls β_p. For remedy, we employ the multisecant and nonlinear GMRES method called Anderson acceleration [19]. As observed in [4], the need for optimized stabilization can be expected to be strongly relaxed, in addition to a generally improved performance.

4 NUMERICAL TESTS

In this section we present the performance of the quasi-Newton schemes with respect to the standard Newton method. We consider the solution of problem (1), whose solution is shown in Figure 2. It can be seen that (i) the base of the geometry allows for free flow of blood and (ii)

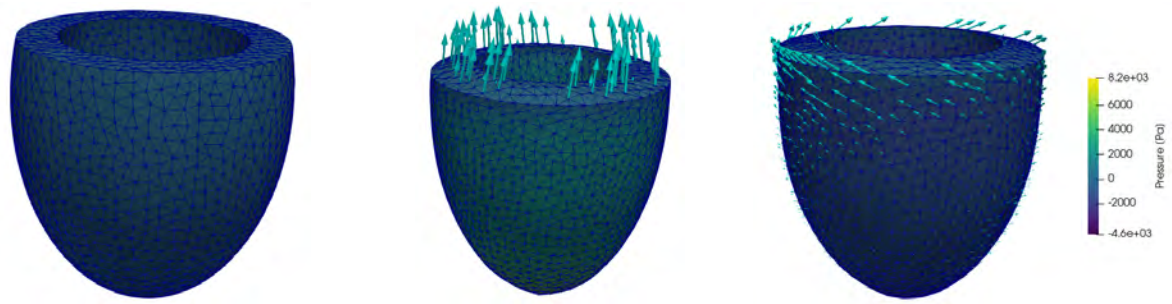

$t = 0.0$ $t = 0.1$ $t = 0.4$

Figure 2: Simulation of the poromechanics model at rest ($t = 0.0$), systole ($t = 0.1$) and dyastole ($t = 0.4$). Deformation is illustrated via the deformation of the geometry, and fluid velocity by the arrows.

it can be seen that the fluid is an absolute velocity, as it follows the heart's untwisting motion during diastole.

To study the splitting schemes we focus on the first 30 time-steps (up to $t = 3 \cdot 10^{-2}$), the mesh used yields around 130 000 degrees of freedom, and all sub-blocks being solved with the GMRES method. We use a right ILU preconditioner with 1 level of fill-in for the splitting methods, and readily highlight that this was not possible for the monolithic Newton solver, as it diverged. For convergence, we required 3 levels of fill-in for the monolithic case. The absolute and relative tolerances used for the linear solvers (GMRES) were 10^{-10} and 10^{-8} for the residual, and instead for the nonlinear solvers (Newton and quasi-Newton) we used 10^{-8} and 10^{-6}, computed through the residual as well. All tests were run in serial to avoid mixing the results with the parallel performance of the precondtioners[1]. The implementation was performed using the FEniCS library [1].

Results are shown in Figure 3, where we depict both the iterations of the nonlinear solvers and the wall-time. We note that Anderson acceleration was fundamental for the convergence of the quasi-Newton schemes, with different levels of depth being required; the depth denotes the amount of previous iterations utilized for determining the next approximation. The two-way split required a depth of at least one, whereas the three-way required a depth of at least 5. It must still be further studied whether the impact of Anderson acceleration is due to an improved robustness with respect to the stabilization parameters as observed in [4] or instead because it improves the convergence of the quasi-Newton itself.

For the iteration counts, cf. Figure 3a, we note that as expected the monolithic Newton method presents a much more robust behavior, with a maximum of three iterations per time-step. The accelerated two-way, albeit with more iterations, also does not present large oscillations in the iteration count, with a minor improvement obtained through further acceleration. The three-way instead varies from 33 to 68 iterations when using 5 levels of acceleration, this behavior being greatly reduced with an acceleration depth of 10, which presents iteration numbers between 31 and 43. This shows the effectiveness of Anderson acceleration in granting robustness to the iterative splitting schemes while the problem character changes over time due to the nonlinearities.

The solution times, cf. Figure 3b, show clearly the superiority of splitting schemes to the monolithic Newton method. The two-way split with one level of acceleration solves each time-step at roughly 15% of the time it takes the monolithic Newton method, whereas the three-way split with 5 levels of acceleration takes in average a 50% of the monolithic time. These times

[1]Simulations were performed in the Indaco cluster from the University of Milan.

can be further improved by means of acceleration, where using an acceleration depth of 10, we see that in average the solution time at each time-step is further reduced to roughly a 10% and a 43% for the two- and three-way respectively, both with respect to the Newton solver.

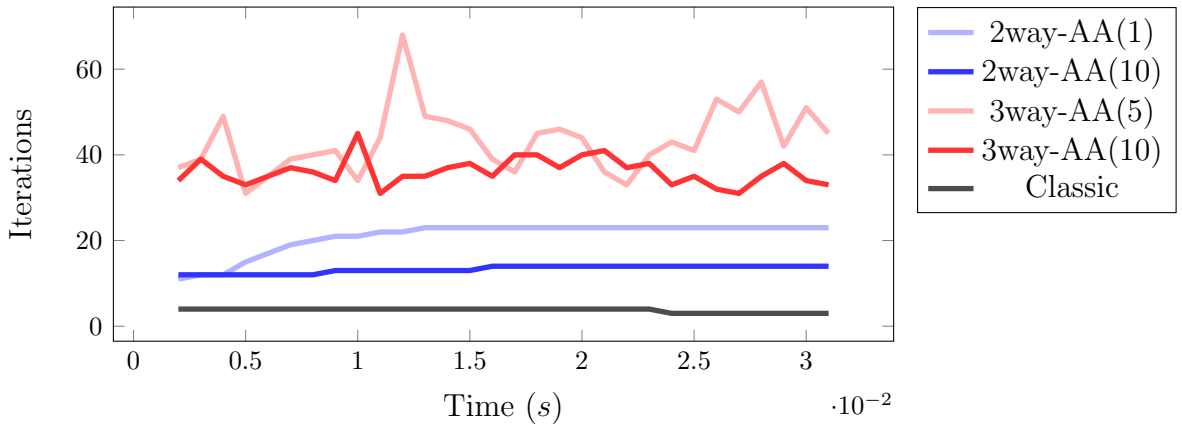

(a) Number of nonlinear solver iterations.

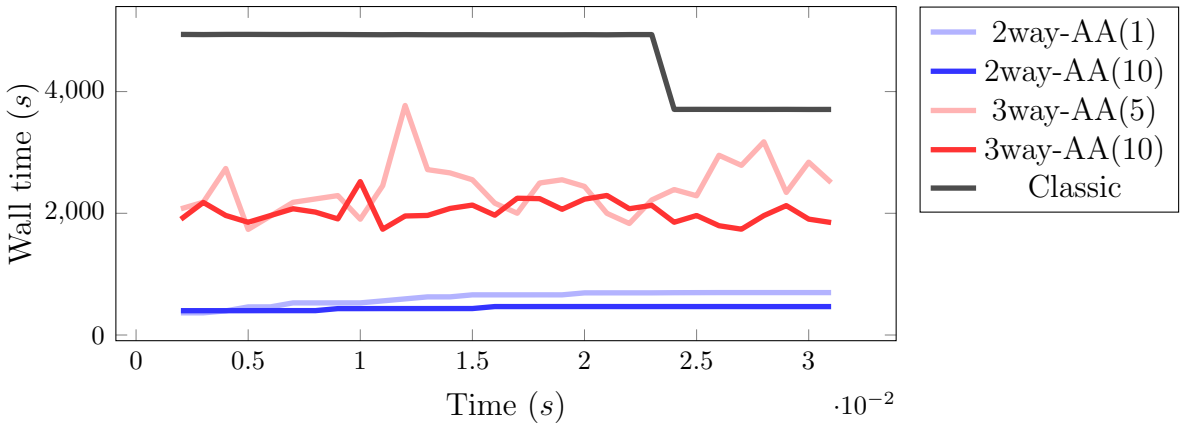

(b) Total solution time.

Figure 3: Iteration counts and solution time at each time step for different nonlinear solvers; depth of Anderson acceleration (AA) in parentheses.

5 CONCLUSIONS

In this work, we have proposed an extension of a two-way splitting scheme for a linearized model presented in [3], now applied as quasi-Newton methods for a nonlinear poroelasticity problem. Both two-way and three-way splitting schemes are considered. Both schemes have been numerically tested for a simplified, nonlinear model of cardiac poromechanics. Our results are very encouraging: the two-way splitting scheme presented an average reduction of the solution time of up to a 85% with respect to the classic Newton scheme, and the three-way a reduction of roughly 50%.

Anderson acceleration provided a crucial improvement to the quasi-Newton methods, without which they would have not converged. The amount of previous iterations required by Anderson depends on the scheme used, 1 being sufficient for the two-way, and instead 5 for the three-way. The three-way splitting scheme, although slightly less performant in this case, presents a more attractive alternative for high performance simulations as it does not require the preconditioning of a saddle point block.

The difference in performance between the monolithic and splitting schemes is mainly justified by the difficulty of devising an efficient preconditioner for the monolithic problem, as can already be seen by the requirement of using additional fill-in with the ILU (1 for the splitting schemes, 3 for the monolithic one). Splitting schemes leverage on the solution of the better understood sub-blocks to yield an overall more efficient solver with potentially better computational complexity.

Future work will be devoted to further investigate three-way decoupling techniques in the context of preconditioning. In addition, the application of quasi-Newton methods inspired by decoupling approaches for the fully nonlinear cardiac poromechanics will be further studied.

6 ACKNOWLEDGEMENTS

The development of this document has been supported by the following projects: "Modeling the heart across the scales: from cardiac cells to the whole organ" PRIN 2017AXL54F_003 P.I. S. Scacchi (NB), Project 250223 Research Council of Norway (JWB), and the FracFlow project funded by Equinor through Akademiaavtalen (JWB). The authors also thank Florin Radu, Paolo Zunino and Alfio Quarteroni for inspiring discussions.

REFERENCES

[1] M. Alnæs, J. Blechta, J. Hake, A. Johansson, B. Kehlet, A. Logg, C. Richardson, J. Ring, M. Rognes, and G. Wells. The FEniCS project version 1.5. *Archive of Numerical Software*, 3(100), 2015.

[2] N. Barnafi, P. Zunino, L. Dedè, and A. Quarteroni. Mathematical analysis and numerical approximation of a general linearized poro-hyperelastic model. *Computers & Mathematics with Applications*, 2020.

[3] J. Both, N. Barnafi, F. Radu, P. Zunino, and A. Quarteroni. Iterative splitting schemes for a soft material poromechanics model. *Computer Methods in Applied Mechanics and Engineering*, 388:114183, 2022.

[4] J. Both, K. Kumar, J. Nordbotten, and F. Radu. Anderson accelerated fixed-stress splitting schemes for consolidation of unsaturated porous media. *Computers & Mathematics with Applications*, 77(6):1479 – 1502, 2019. 7th International Conference on Advanced Computational Methods in Engineering (ACOMEN 2017).

[5] J. W. Both, K. Kumar, J. M. Nordbotten, and F. A. Radu. Iterative methods for coupled flow and geomechanics in unsaturated porous media. In *Poromechanics VI*, pages 411–418. 2017.

[6] B. Burtschell, D. Chapelle, and P. Moireau. Effective and energy-preserving time discretization for a general nonlinear poromechanical formulation. *Computers and Structures*, 182:313–324, 2017.

[7] B. Burtschell, P. Moireau, and D. Chapelle. Numerical analysis for an energy-stable total discretization of a poromechanics model with inf-sup stability. *Acta Mathematicae Applicatae Sinica*, 35(1):28–53, 2019.

[8] J. Cahouet and J.-P. Chabard. Some fast 3d finite element solvers for the generalized stokes problem. *International Journal for Numerical Methods in Fluids*, 8(8):869–895, 1988.

[9] D. Chapelle, J. Gerbeau, J. Sainte-Marie, and I. Vignon-Clementel. A poroelastic model valid in large strains with applications to perfusion in cardiac modeling. *Computational Mechanics*, 46(1):91–101, 2010.

[10] D. Chapelle and P. Moireau. General coupling of porous flows and hyperelastic formulations - from thermodynamics principles to energy balance and compatible time schemes. *European Journal of Mechanics, B/Fluids*, 46:82–96, 2014.

[11] A. Cookson, J. Lee, C. Michler, R. Chabiniok, E. Hyde, D. Nordsletten, M. Sinclair, M. Siebes, and N. Smith. A novel porous mechanical framework for modelling the interaction between coronary perfusion and myocardial mechanics. *Journal of biomechanics*, 45(5):850–855, 2012.

[12] A. Gerbi, L. Dedè, and A. Quarteroni. A monolithic algorithm for the simulation of cardiac electromechanics in the human left ventricle. *Mathematics In Engineering*, 1(1):1–37, 2019.

[13] J. Guccione, A. McCulloch, and L. Waldman. Passive material properties of intact ventricular myocardium determined from a cylindrical model. *Journal of biomechanical engineering*, 113(1):42–55, 1991.

[14] J. Huyghe, T. Arts, D. van Campen, and R. Reneman. Porous medium finite element model of the beating left ventricle. *American Journal of Physiology-Heart and Circulatory Physiology*, 262(4):H1256–H1267, 1992.

[15] M. A. B. Reverón, K. Kumar, J. M. Nordbotten, and F. A. Radu. Iterative solvers for biot model under small and large deformations. *Computational Geosciences*, 25(2):687–699, 2021.

[16] A. Settari and F. Mourits. A coupled reservoir and geomechanical simulation system. *SPE Journal*, 3(3):219–226, 1998.

[17] E. Storvik, J. W. Both, K. Kumar, J. M. Nordbotten, and F. A. Radu. On the optimization of the fixed-stress splitting for biot's equations. *International Journal for Numerical Methods in Engineering*, 120(2):179–194, 2019.

[18] T. Usyk, I. LeGrice, and A. McCulloch. Computational model of three-dimensional cardiac electromechanics. *Computing and Visualization in Science*, 4(4):249–257, Jul 2002.

[19] H. F. Walker and P. Ni. Anderson acceleration for fixed-point iterations. *SIAM Journal on Numerical Analysis*, 49(4):1715–1735, 2011.

[20] S. Whitaker. Flow in porous media i: A theoretical derivation of darcy's law. *Transport in porous media*, 1(1):3–25, 1986.

[21] O. Zienkiewicz, D. Paul, and A. Chan. Unconditionally stable staggered solution procedure for soil-pore fluid interaction problems. *International Journal for Numerical Methods in Engineering*, 26(5):1039–1055, 1988.